



CHARACTERIZATION OF ELECTRICAL PROPERTIES OF 3D PRINTED BIOSENSORS WITH VARIOUS ELECTRODE GEOMETRIES

SORINA GOGONEAȚĂ¹, CĂTĂLIN MĂRCULESCU², ALEXANDRU M. MOREGA^{3,4}

Keywords: Electrochemical biosensors; 3D printing; Electrodes; Electrode geometry; Electrochemical impedance spectroscopy.

This study explores the design and fabrication process of 3D-printed electrodes for electrochemical biosensors that detect ion concentration. The 3D printing process enables the production of electrodes with complex shapes. To determine their performance, cyclic voltammetry, and electrochemical impedance spectroscopy were used to test the electrodes' ability to detect changes in ion concentration. The results reveal the impact of electrode geometry on biosensor performance.

1. INTRODUCTION

Electrochemical biosensors are advanced instruments for detecting or sensing analytes that have biological or environmental importance. Over the past few years, electrochemical biosensors have become increasingly popular as a viable option for clinical diagnostic devices, particularly for infectious diseases and health monitoring. These sensors employ various detection methods, including DNA events, enzyme-substrate interactions, antibody-antigen interactions, pH changes, specific ions, or molecules in a sample, or redox reactions to generate electrochemical signals [1]. They can be used as portable or wearable devices in laboratory settings, making them a valuable tool with great flexibility for healthcare monitoring [2].

In recent years, the increasing demand for point-of-care testing and personalized medicine led to the development of innovative biosensors and manufacturing techniques. One technique that gained significant attention is 3D printing with biocompatible materials because of its potential applications in medicine, tissue engineering, and regenerative medicine [3].

The fabrication of electrodes traditionally relies on conventional techniques like screen printing and photolithography. These conventional approaches are labor-intensive, require cleanroom processing, and involve multiple steps using toxic materials [4].

Compared to conventional manufacturing techniques, 3D printing enables the creation of various objects with high precision and accuracy, using a digital model designed explicitly for a particular system. In the field of electrochemical applications such as electrochemical biosensors, carbon-based materials are the most frequently utilized. In 3D printing, these materials are used as ink or paste for electrode fabrication and involve the combination of carbon allotropes to create hybrid materials [3, 5].

Carbon-based materials such as carbon nanotubes [6], carbon fibers [7], carbon black [8, 9], graphene [10], and graphene oxide [11, 12] are among the most commonly used materials in 3D printing because of their unique properties.

The most notable property of these carbon-based materials is their high conductivity enabling efficient charge transfer and electron transport, making them suitable for various applications in electronics, sensing, and electrochemical devices [13]. Carbon-based materials possess good

mechanical properties, including flexibility and resilience, without compromising electrical performance. This combination of electrical and mechanical properties makes carbon-based materials highly desirable for applications such as wearable devices and flexible electronics [9].

In recent years, the use of 3D printing for fabricating electrochemical sensors and biosensors has gained significant importance, providing better precision and control in designing and producing sensor structures [14].

One of the main benefits of 3D printing technologies is their ability to facilitate rapid prototyping, minimize costs, enable miniaturization, and allow for design customization, providing the option of using hybrid materials. Additionally, the capability for multi-material 3D printing makes it possible to easily create diverse structures based on varying material and geometry properties [12].

With computer-aided design (CAD) software, the 3D printing technique creates a wide range of electrode geometries with high precision.

Various factors, including its geometry, influence the electrical properties of an electrode. Increasing the surface area of an electrode has been observed to enhance its electrical conductivity, as it provides more pathways for electron flow. Consequently, the overall resistance of the electrode is reduced [15].

This article aims to study the design and fabrication process of 3D-printed electrodes for electrochemical biosensors and analyze their electrical properties using electrochemical impedance spectroscopy, EIS.

2. DESIGN AND FABRICATION

In electrochemical biosensors, the design and fabrication of electrodes are critical issues in achieving accurate and sensitive detection of target analytes. The development of 3D printing technologies has enabled the creation of electrodes with customized geometries and improved performance.

The advantages of 3D printing of electrodes are the speed of the process, reduced costs, and reasonable control of electrode geometry using materials compatible with biological samples.

2.1 DESIGN CONSIDERATIONS (ELECTRODE GEOMETRY)

A typical electrochemical biosensor comprises three main elements: a working electrode, a reference electrode with a

¹ Doctoral School of Electrical Engineering, University POLITEHNICA of Bucharest, Bucharest, Romania, E-mail: s.gogoneata@gmail.com

² National Institute for Research and Development in Microtechnologies—IMT Bucharest, E-mail: catalin.marculescu@imt.ro

³ Faculty of Electrical Engineering, University POLITEHNICA of Bucharest, Bucharest, Romania, E-mail: alexandru.morega@upb.ro

⁴ "Gh. Mihoc – C. Iacob" Institute of Statistical Mathematics and Applied Mathematics, Romanian Academy, Bucharest, Romania

known potential, and a counter electrode, as shown in Fig. 1. The active electrode is where the sensing material and the target analyte interact, leading to a change in the electrical properties that are measurable. The size and shape of the working electrode can significantly influence the sensitivity and response time of the biosensor.

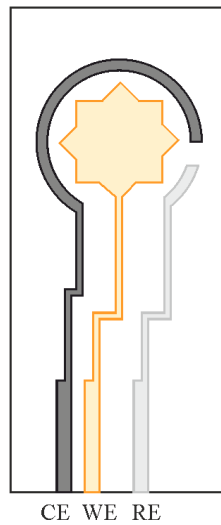


Fig. 1 – An electrochemical biosensor with a three electrodes configuration

For a better understanding of the electrode geometry's role, several patterns are presented in Fig. 2.

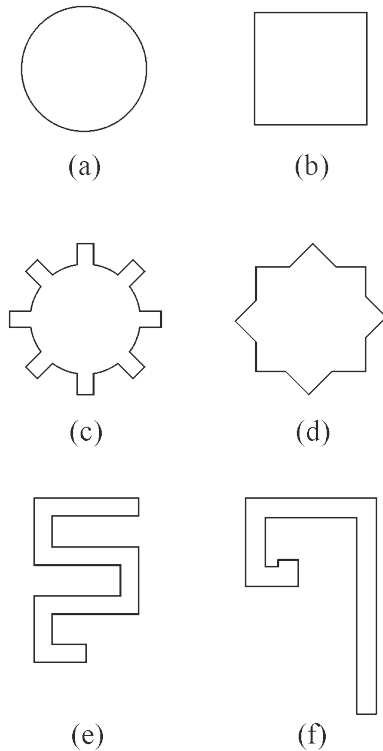


Fig. 2 – Different shapes of working electrodes: a) Circle; b) Square; c) Gear; d) Star; e) S-shaped pattern; f) Fibonacci [16]

The electrode may have different shapes, such as circles, squares, gears, stars, S-shapes, and Fibonacci patterns.

The *circular* shape has a diameter of 4 mm, which represents the distance across the circle passing through its center, Fig. 2.a. The *square* shape, Fig. 2.b, has a 4 mm edge length. The *gear* shape is defined by its diameter, measured from one outer edge to the opposite outer edge, 5.6 mm. The

gear consists of 8 teeth, 0.6 mm in width and 0.8 mm in length, Fig. 2.c. The *star* shape features 8 peaks, each at 90-degree angle, and the length of each peak's edge is 1.17mm. This configuration creates a symmetrical pattern, with the peaks evenly distributed around the center, Fig. 2.d. The *S-shaped* structure is created by merging two mirrored “C” shapes in a curving wave-like pattern. The upper part of the S-curve curves to the left, while the lower part curves to the right, giving it a distinct serpentine appearance. The dimensions of the S-shaped structure are 4 mm in width and 6 mm in length, Fig. 2.e. The working electrode with a *Fibonacci* shape was designed using a Fibonacci sequence of 8, 5, 3.3, 2, 1, and 0.8 mm for its' edges, Fig. 2.f. The WE geometry surfaces are presented in Table 1:

Table 1
Working electrode geometry surface

Geometry	mm ²
Circular	12.5
Square	16
Gear	16.4
Star	18.7
S-shaped pattern	10.5
Fibonacci	12.8

2.2. THE METHOD OF FABRICATION

In 3D bioprinting, the fabrication of electrodes typically involves using specialized bioprinters that deposit conductive materials layer by layer to form the desired geometry. There are several techniques for 3D bioprinting electrodes, including extrusion-based printing, inkjet-based printing, and laser-assisted printing [11].

Extrusion-based printing involves extruding a conductive paste or ink through a nozzle to create the desired pattern. It is important to note that the specific fabrication process used for these electrodes was initially developed and implemented as part of a previous work [14].

This technique allows for precise control over the material deposition, making it suitable for printing complex geometries. However, the conductive material's viscosity can limit the printed electrodes' resolution and accuracy.

In the field of bioprinting, the quality and characteristics of the substrate are essential for successful printing of 3D structures. The substrate must be impurity-free and have a suitable surface for the carbon-based ink to adhere to.

Therefore, a cleaning process is necessary before printing, using isopropanol and air jets to remove particles from the surface. The substrate is then attached to the bioprinter platform, and the printing process may be initiated [14].

2.2.1. THE SUBSTRATE

A 50 μm thick polyimide (Kapton®) adhesive sheet was used to fabricate the electrode. The sheet was carefully shaped to 25 \times 10 mm and then attached to a solid support substrate with identical dimensions.

Kapton possesses good qualities that make it suitable for biosensing applications, including high temperature and chemical resistance and favorable dielectric properties [17].

To ensure that the Kapton tape is applied without any air bubbles or wrinkles, it is necessary to use a flat and uniform surface for solid support. The solid support utilized is a silicon wafer cut to the required size.

2.2.2. CARBON-BASED INK

A highly conductive carbon-based ink with high viscosity (250–300 Pa. s, CH-8, Jelcon Corp., Tokyo, Japan) was used in printing complex electrode geometries. The high viscosity

of the ink allows it to maintain its shape and adhere well to the printing substrate during the 3D printing process.

Additionally, it is biocompatible and suitable for use in biosensors and other biomedical applications [17]. The syringe containing it is loaded into the dispensing system of the bioprinter, which controls the flow of the ink and allows for precise deposition onto the printing substrate, enabling the creation of intricate electrode structures with high conductivity.

2.2.3. PRINTING PARAMETERS

The following printing parameters were used for the extrusion operation:

Extrusion pressure (p) is essential in determining the pressure applied to the material during the extrusion process. In this case, a pressure of 5 bars was utilized for the carbon ink.

Head print speed controls how fast the printer moves when laying down the material, and it was set in a range from 10 to 20 mm/s for the carbon ink.

The layer height refers to the thickness of each printed layer, ranging from 100 to 200 microns.

2.1.1. CREATING THE G-CODE FILE

The electrode geometries are designed in computer-aided design (CAD) software and then converted into G-code files by following several steps [18]. To prepare the CAD file for 3D printing, the electrode is first converted to a standard 3D printing format and then loaded into slicing software, where it is sliced into 2D layers. The G-code file contains instructions for the printer, such as the print head's movement and the nozzle's temperature. This file is transferred to the 3D printer, which reads the instructions and prints the object.

2.3.3. POST-PROCESSING

Thermal treatment can be carried out to improve the conductivity and stability of the printed electrodes by drying the ink more efficiently. To achieve this, the electrodes were subjected to a short, 30-minute heat treatment at 140 °C using a heating plate, as shown in Fig. 3.



Fig. 3 – Heating plate.

Additionally, the electrodes can be functionalized or coated with a material to enhance their performance based on the intended application.

3. ELECTROCHEMICAL CHARACTERIZATION

3.1 APPARATUS AND TEST SETUP

A potentiostat is utilized to manage the electrochemical potential applied to the electrodes and to measure the resulting electrical signals while analyzing the electrodes' electrochemical properties.

The Nova 2.1.6 software was employed to conduct all electrochemical studies performed in this research, using the Autolab PGSTAT204 potentiostat equipped with a FRA32M electrochemical impedance spectroscopy (EIS) module (METROHM AUTOLAB AG, Utrecht, The Netherlands).

One of its standard configurations is the 3-electrode setup, which consists of a *working electrode*, a Metrohm standard LL-Ag/AgCl *reference electrode*, and a Metrohm standard platinum sheet *counter electrode*, Fig. 4.



Fig. 4 – retort stand for 3-electrode cell configuration: a) 3D printed electrode (WE); b) redox solution; c) (CE); d) (RE)

Using a 3-electrode configuration, the working electrode's potential can be accurately controlled and measured relative to the reference electrode. In contrast, the counter electrode provides a continuous supply of electrons to support the electrochemical reaction.

The potential applied to the working electrode causes the analyte to suffer an oxidation or reduction reaction, which generates an electrical current that the potentiostat can measure.

By monitoring the electrical current generated by the oxidation or reduction of the ferrocyanide ions at the working electrode, important electrochemical properties such as the electron transfer rate, the electrode surface area, and the kinetics of the reaction can be studied.

Six different designs of printed electrodes were experimented with, Fig. 5, to determine the optimal electrical parameters. Carbon-based ink was also used to create electric routes and pads.

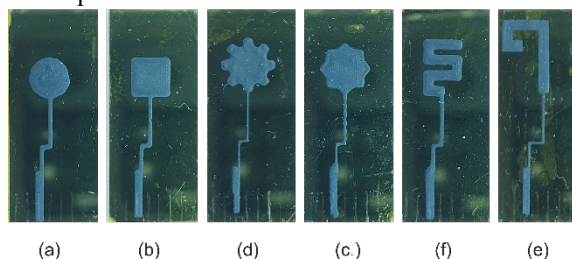


Fig. 5 – Working electrodes geometries: a) Circle; b) Square; c) Gear; d) Star; e) S-shape pattern; f) Fibonacci.

3.2 EXPERIMENTAL CONDITIONS

3.2.1. THE SOLUTION

The experiments were performed on 3D-printed working electrodes immersed in an electrolyte containing potassium ferrocyanide ($K_4[Fe(CN)_6]$) in a supporting electrolyte which allows for the electrochemical reactions to take place at the surface of the working electrode.

Potassium ferrocyanide is known for its redox activity, meaning it can undergo both oxidation and reduction reactions, which are reversible. The solution is stable, it has good electrical conductivity, making it suitable for various electrochemical analysis techniques.

3.3 ELECTRICAL MEASUREMENTS

Applying cyclic voltammetry and impedance spectroscopy enables the investigation of how the distinct geometries influence the electrodes' functionality and can help optimize their design for specific applications

The Autolab PGSTAT204 potentiostat can measure various parameters in cyclic voltammetry (CV), including the potential at which the redox reaction occurs, the peak current of the oxidation or reduction, and the scan rate. These parameters can provide information about the electrochemical behavior and properties of the working electrode, such as its electroactive surface area, the kinetics of electron transfer, and the stability of the electrode surface.

The parameters measured in electrochemical impedance spectroscopy (EIS) include: the impedance magnitude and phase angle, the real and imaginary components of impedance, and other electrochemical parameters such as charge transfer resistance, double-layer capacitance, and Warburg impedance may be deduced.

4. RESULTS

Electrochemical impedance spectroscopy allows for the non-destructive examination of biosensors' properties.

A conventional three-electrode EIS method was used to study the impact of the working electrode's geometry on biosensors' performances. Various configurations of electrode area were exposed to the electrolyte as an active area for the investigation. The experiments used a frequency range from 0.1 Hz to 100 kHz for all tests. The working electrode exposed to the electrolyte was connected to the potentiostat through a data port.

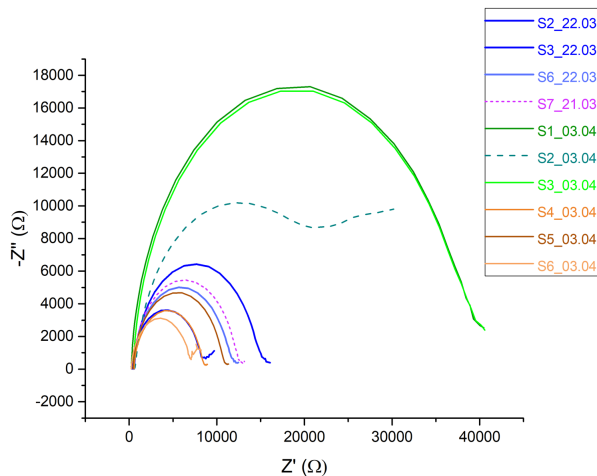


Fig. 6 – Nyquist plot for impedance response – Table 2.

The impedance response was observed using potassium ferrocyanide as the electrolyte. Six different active areas of the

working electrode were used to vary the active area of the working electrode. Figure 6 presents the Nyquist plot for impedance response that shows the surface and volume diffusion competition coupled with the electric charge exchange processes [19, 20]. From the data obtained from the Nyquist plot, an equivalent circuit model for a biosensor is created, Fig. 7.

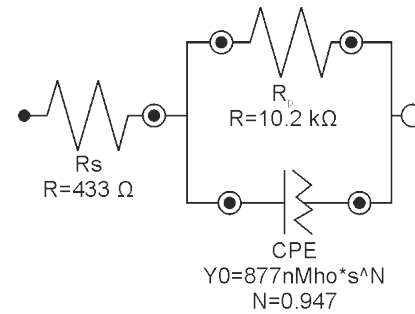


Fig. 7 – Randles circuit for S5_03.04.2023 electrode.

The charge transfer resistance (R_{ct}), polarization resistance (R_p), maximum imaginary impedance (Z''_{max}), the maximum phase difference between current and voltage (ϕ_{max}), double-layer capacitance (C_{dl}), and constant-phase element (CPE) were determined for each setup, Table 2.

Table 2
Working electrode electrical properties

	ϕ_{max}	Z''_{max} [Ω]	R_{ct} [Ω]	R_p [Ω]	C_{dl} [μF]	Y_0 [CPE]	N
S1_03.04 Circle	77.48	17308	20660	40474	3.07	1.51E-06	0.94
S3_03.04 Circle	73.65	17035	17279	40600	2.91	1.51E-06	0.94
S2_03.04 Circle	64.30	10189	11933	20722	6.69	3.61E-06	0.91
S2_22.03 Fibonacci	63.62	6434	7677	15451	2.61	1.40E-06	0.94
S7_21.03 Gear	64.68	5460	6453	13020	1.96	1.04E-06	0.95
S5_03.04 Square	62.90	4670	6027	11187	1.67	8.77E-07	0.95
S6_22.03 Star	63.06	5014	5658	12400	2.81	1.53E-06	0.94
S3_22.03 ZigZag	63.88	3609	4434	8457	1.80	9.57E-07	0.93
S4_03.04 Square	57.52	3573	4014	8760	1.58	9.13E-07	0.95
S6_03.04 Square	65.13	3118	3579	7056	1.77	9.50E-07	0.96

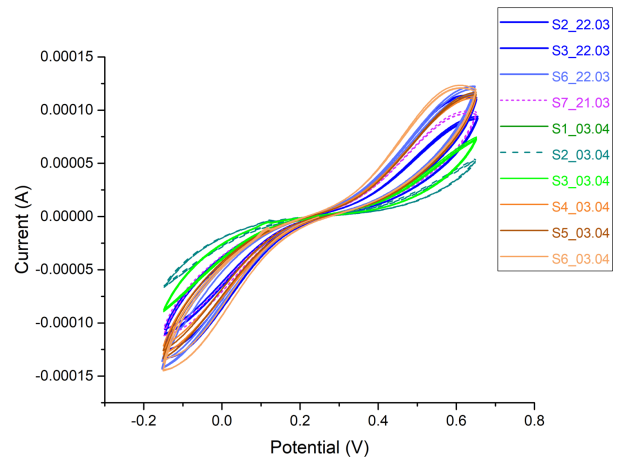


Fig. 8 – Cyclic voltammetry plot for the sensors listed in Table 2.

The correlation between current intensity and potential for the 10 different working electrodes that were tested is

illustrated in Fig. 8 in a cyclic voltammetry plot. During the analysis, it was observed that both oxidation and reduction peaks were present in the cyclic voltammogram. However, it should be noted that the positions of these peaks were not identical for each working electrode. There were slight variations in the peak positions, indicating differences in the electrochemical behavior of the electrodes.

The phase difference (φ), constant phase element admittance Y_{CPE} , and N number are sensitive to the system parameters, thus efficiently comparing the theoretical model with the experiment. The CV scan was performed using a potential window $[-0.4, 0.4]$ V, with a scan rate of 100 mV/s.

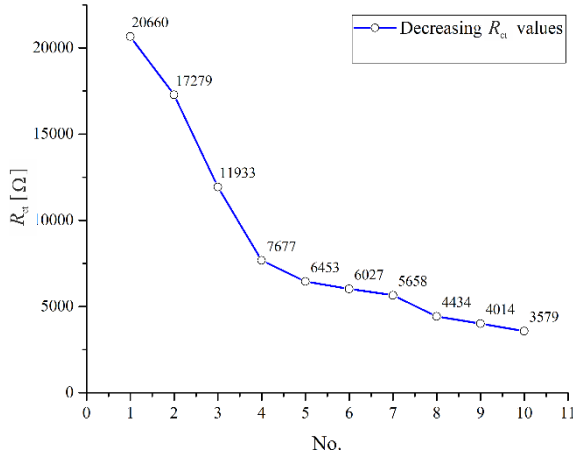


Fig. 9 – R_{ct} variation plot for the sensors listed in Table 2.

The experimental results indicated that circular-shaped electrodes, with the highest R_{ct} values, as shown in Fig. 9, exhibited a slower charge transfer than square-shaped electrodes, with the lowest R_{ct} values. This slower charge transfer can reduce sensitivity, requiring higher potential or longer measurement times to achieve a measurable response or detect analytes.

5. DISCUSSION OF RESULTS

Our study initially aimed to investigate and characterize the electrical properties of 3D bio-printed biosensors with different working electrode geometries. We conducted analyses to evaluate and understand how the geometric features of electrodes influence their electrical performance.

To achieve this, we fabricated electrodes of different shapes, sizes, and configurations and conducted electrical characterization using techniques like electrical impedance spectroscopy and cyclic voltammetry.

We utilized the standard counter and reference electrodes from the electrochemical cell of the Autolab PGSTAT204 potentiostat. To establish a connection between each printed working electrode and the potentiostat, we utilized an 8-pin SATA port.

We focused on printing only the working electrode and its associated electric routes and pads to facilitate fabrication. This approach simplified the process and reduced the fabrication. We opted for cost-effective materials like Kapton and carbon-based ink.

The resistance of an electrode can be affected by its dimensions. A longer and thinner electrode will have a higher resistance than a shorter and thicker one. This is because resistance is proportional to length and inverse to the cross-sectional area, as Ohm's law states.

The potential applied to the working electrode causes the analyte to suffer an oxidation or reduction reaction, which

generates an electrical current that the potentiostat can measure.

By monitoring the electrical current generated by the oxidation or reduction of the ferrocyanide ions at the working electrode, important electrochemical properties such as the electron transfer rate, the electrode surface area, and the kinetics of the reaction can be studied.

Increasing the surface area of the biosensor can enhance analyte capture and increase detection sensitivity.

The configuration of electrodes, ranging from simple shapes like circles or squares to more complex structures like gears or Fibonacci shapes, influences how electrical fields are distributed, and analytes interact with the electrodes.

Efficient geometries and optimized electrical properties can lead to faster response times, enabling real-time or near-real-time monitoring.

While our methodology proved successful in achieving our research goals, it is essential to acknowledge some potential limitations:

- we only examined a limited range of working electrode geometries. Other geometries, which might have different electrical properties and performance characteristics, are worth investigating.

- the observed electrical properties of the biosensors may be influenced by experimental conditions such as temperature, electrolyte concentration, and electrode polarization.

6. CONCLUSIONS

The preliminary findings of our study have shown promising results, particularly in the application of electrochemical impedance spectroscopy (EIS) and the analysis of Nyquist diagrams.

The results highlight the crucial role of the electrodes' shape and surface area in determining the charge transfer efficiency. As observed in square-shaped electrodes, larger surface areas demonstrated more efficient charge transfer than circular-shaped electrodes.

In conclusion, the square-shaped electrode design yields the lowest resistance values, suggesting it is the optimal choice. Therefore, the square shape demonstrates superior performance in terms of R_{ct} value.

Further research in 3D-printed biosensors could focus on integrating simulation and mathematical modeling techniques to complement experimental studies. Additionally, integrating simulation results with experimental data can provide valuable insights into the behavior of 3D-printed electrodes for biosensors under different conditions, improving their reliability and practical applications.

ACKNOWLEDGEMENTS

This work was conducted in the Laboratory for Micro- and Nano-Fluidics, National Institute for Research and Development in Microtechnologies. The support provided by Dr. Marioara Avram is gratefully acknowledged.

The financial support offered by the Ministry of Investments and European Projects through the Human Capital Sectoral Operational Program 2014-2020, Contract no. 62461/03.06.2022, SMIS code 153735, is also acknowledged.

Received on 27 May 2023

REFERENCES

1. J.I.A. Rashid, N.A. Yusof, *The strategies of DNA immobilization and hybridization detection mechanism in the construction of electrochemical DNA sensor: A review*, *Sens. Bio-Sensing Res.*, **16**, pp. 19–31 (2017).
2. H.A. Abdulbari, E.A.M. Basheer, *Electrochemical biosensors: electrode development, materials, design, and fabrication*, *ChemBioEng Rev.*, **4**, 2, pp. 92–105 (2017).
3. J. Contreras, V. Perez-Gonzalez, M. Mata, O. Aguilar, *3D-printed hybrid-carbon-based electrodes for electroanalytical sensing applications*, *Electrochem. commun.*, **130**, p. 107098 (2021).
4. D. Dăscălescu, C. Apetrei, *Development of a novel electrochemical biosensor based on organized mesoporous carbon and laccase for the detection of serotonin in food supplements*, *Chemosensors*, **10**, 9, p. 365 (2022).
5. L.R. Silva, A. Gevaerd, L. Marcolino Jr., M. Bergamini, T. Almeida Silva, B. Janegitz, *3D-printed electrochemical devices for sensing and biosensing of biomarkers*, *Advances in Bioelectrochemistry*, **2**, pp. 121–136 (2022).
6. H. Wei, X. Cauchy, I. O. Navas, Y. Abderrafai, K. Chizari, U. Sundararaj, Y. Liu, J. Leng, D. Therriault, *Direct 3D printing of hybrid nanofiber-based nanocomposites for highly conductive and shape memory applications*, *ACS Appl. Mater. Interfaces*, **11**, 27, pp. 24523–24532 (2019).
7. S.H.R. Sanei, D. Popescu, *3D-printed carbon fiber reinforced polymer composites: a systematic review*, *J. Compos. Sci.*, **4**, 3, 98 (2020).
8. C. Callanan, L. Hsu, A. McGee, *Formulation and evaluation of carbon black 3D printing materials*, *OCEANS 2018 MTS/IEEE Charleston* (2018).
9. Y. Zheng, X. Huang, J. Chen, K. Wu, J. Wang, X. Zhang, *A review of conductive carbon materials for 3D printing: materials, technologies, properties, and applications*, *Materials*, **14**, 14, p. 3911 (2021).
10. Z.C. Kennedy, J.F. Christ, K.A. Evans, B.W. Arey, L.E. Sweet, M.G. Warner, R.L. Erikson, C. A. Barrett, *3D-printed poly (vinylidene fluoride)/carbon nanotube composites as a tunable, low-cost chemical vapour sensing platform*, *Nanoscale*, **9**, 17, pp. 5458–5466 (2017).
11. H. Guo, R. Lv, S. Bai, *Recent advances on 3D printing graphene-based composites*, *Nano Mater. Sci.*, **1**, 2, pp. 101–115 (2019).
12. L.R.G. Silva, J.S. Stefano, L.O. Orzari, L.C. Brazaca, E. Carrilho, L.H. Marcolino-Junior, M.F. Bergamini, R.A. A. Munoz, B.C. Janegitz, *Electrochemical biosensor for SARS-CoV-2 cDNA detection using aups-modified 3D-printed graphene electrodes*, *Biosensors*, **12**, p. 622 (2022).
13. C. Wang, K. Xia, H. Wang, X. Liang, Z. Yin, Y. Zhang, *Advanced carbon for flexible and wearable electronics*, *Adv. Mater.*, **31**, 9, p. 1801072 (2019).
14. C. Marculescu, P. Preda, T. Burinaru, E. Chiriac, B. Tincu, A. Matei, O. Brincoveanu, C. Pachiu, M. Avram, *Customizable fabrication process for flexible carbon-based electrochemical biosensors*, *Chemosensors*, **11**, 4, p. 204 (2023).
15. S. Handaja, H. Susanto, H. Hermawan, *Electrical conductivity of carbon electrodes by mixing carbon rod and electrolyte paste of spent battery*, *Int. J. Renew. Energy Dev.*, **10**, 2, pp. 221–227 (2021).
16. S.J. Bharathi, S.H. Thilagar, V. Jayasurya, *Design of electrochemical sensor and determining the peak current of ions in solution*, *IEEE International Conference on Intelligent Techniques in Control, Optimization and Signal Processing (INCOS)*, pp. 1–4, (2019).
17. M. Xu, D. Obodo, V.K. Yadavalli, *The design, fabrication, and applications of flexible biosensing devices*, *Biosens. Bioelectron.*, **124–125**, pp. 96–114 (2019).
18. A. Ambrosi, A. Bonanni, *How 3D printing can boost advances in analytical and bioanalytical chemistry*, *Microchim. Acta*, **188**, 8, p. 265 (2021).
19. B. Tincu, T. Burinaru, A.-M. Enciu, P. Preda, E. Chiriac, C. Marculescu, M. Avram, A. Avram, *Vertical graphene-based biosensor for tumor cell dielectric signature evaluation*, *Micromachines*, **13**, 10, p. 1671 (2022).
20. T. A. Burinaru, B. Tincu, M. Avram, P. Preda, A.-M. Enciu, E. Chiriac, C. Mărculescu, T. Constantin, M. Militaru, *Electrochemical impedance spectroscopy based microfluidic biosensor for the detection of circulating tumor cells*, *Mater. Today Commun.*, **32**, p. 104016 (2022).